Lattice-Boltzmann Simulations of Delta Wings – VFE-2 and SACCON

Erol Özger
Technische Hochschule Ingolstadt, Esplanade 10, 85049 Ingolstadt
GERMANY

erol.oezger@thi.de

Benedikt Koenig, André F.P. Ribeiro, Davide Cerizza, Ehab Fares
Dassault Systèmes – SIMULIA, Curiestrasse 4, 70563 Stuttgart
GERMANY

benedikt.koenig@3ds.com, andre.ribeiro@3ds.com, ehab.fares@3ds.com, davide.cerizza@3ds.com

ABSTRACT

The Lattice-Boltzmann code PowerFLOW is used to simulate the academic VFE-2 and the realistic SACCON delta wing configurations. The first is a generic simple delta wing geometry with only sharp leading edges containing the fundamental flow features of such cases, namely the primary and secondary leading edge vortices. The SACCON configuration has a more complex shape with sharp and rounded leading edges producing a very non-linear flow behavior highlighted in the moment coefficient polar. This behavior is expected to be challenging to capture in simulation. Results of the computations agree fairly well with available experimental data, indicating that the current approach can be used for other similar realistic configurations.

1.0 INTRODUCTION

Delta wing flows at increasing angles-of-attack are characterized by the generation of strong detached leading edge vortices making up the well-known additional non-linear lift contribution to the linear contribution generated by bound vorticity. The leading edge vortex is more a system of vortices detached above the wing consisting of a strong primary vortex and a weaker secondary vortex with counter rotation. Since delta wings have very beneficial low and high speed properties they are vastly used in the design of fighter aircraft.

The vortical flows associated with delta wing configurations are closely related to the fundamental issue of flow separation. Numerical simulation of these phenomena is non-trivial due to the potentially close interaction between modelling the separation point and the feedback from detached flow to the boundary layer [1]. Current state-of-the-art Reynolds-Averaged Navier-Stokes (RANS) tools have been applied to these flows in the past with some success, but their reliable application is typically limited by their known shortcomings in handling turbulent separated flows. Better suited Navier-Stokes-based methods, such as Large Eddy Simulations (LES) and hybrid RANS/LES, have not reached the level of efficiency and/or reliability that would be required for industrial application [1].

As an alternative to these Navier-Stokes methods, the Lattice-Boltzmann method (LBM) has recently been shown to complement current Computational Fluid Dynamics (CFD) tools for flows that are largely dominated by separated or vortical flows. LBM itself is considered a novel non-traditional CFD technique [1] that offers a number of valuable capabilities beyond the classical Navier-Stokes based methods. Some of the most interesting features of this method for the current application include the capabilities to automatically mesh arbitrarily complex geometries, to easily increase resolution locally in areas of

interesting small scale geometric or flow features, to efficiently treat highly unsteady flows, and to handle largely different velocity scales with low numerical dissipation. That makes the method well suited to simulate realistic vehicle configurations with all their geometrical complexity at extreme flow conditions where large flow separations occur.

In this work, the LBM tool PowerFLOW is used to simulate two different delta wing configurations, the well-known VFE-2 [2] and the SACCON [3], which could more accurately be described as a lambda wing. The VFE-2 model will be used in its sharp leading edge configuration, to validate the method for the prediction of the primary and secondary vortical structures. The SACCON serves here as a more realistic model, representing a highly maneuverable UCAV. It features a lambda shape with a mixed leading edge, blending between sharp and rounded regions.

2.0 NUMERICAL METHOD

LBM is a CFD technology developed over the last 30 years [4, 5], which has been validated for a wide variety of applications ranging from academic Direct Numerical Simulation (DNS) cases [6] to industrial flow problems in the fields of aerodynamics [7, 8, 9] and aeroacoustics [10, 11]. Its motivation is to simulate a fluid derived from a microscopic level where the physics are simpler and more general [12] than the macroscopic continuum approach taken by the Navier-Stokes equations. The latter can, however, be recovered from the LBM under certain conditions [13]. The unsteady nature of the LBM solution with low numerical dissipation makes the code especially well-suited for problems involving multi-scale turbulent separated flows. The code offers a highly efficient local implementation of the LBM algorithm suitable for scalable distributed computations on thousands of processors.

The Lattice Boltzmann flow simulation is equivalent to a DNS of the flow. For high Reynolds number, such as those addressed in this work, the Lattice Boltzmann Very Large Eddy Simulation (LB-VLES) approach [14, 15] is used. It is conceptually similar to hybrid RANS/LES methods where especially high Reynolds (Re) number boundary layers are modelled while off-body larger turbulent flow structures within separated regions are resolved with low dissipation. To reduce the resolution requirements near the wall for high Re flows, a hybrid wall function including compressibility effects is used to model the region of the boundary layer closest to the solid surfaces.

The Lattice Boltzmann approach is solved on Cartesian meshes, which are generated automatically for any geometrically complex shape. Variable refinement regions (VR) can be defined to allow for local mesh refinement of the grid by successive factors of two. A more detailed description of the numerical method is given in [16].

3.0 RESULTS

This section is split into two parts: the first documents the results and comparisons with experiments of the VFE-2 and the second of the SACCON configuration.

3.1 VFE-2 DELTA WING CONFIGURATION

Results for the VFE-2 model with the sharp leading edge and 65° leading edge sweep, corresponding to the conditions tested at TU Munich [2] are presented here. The Reynolds number is $1x10^6$ and the Mach number is 0.07. Figure 12-1 shows the case at an angle-of-attack α=13° with developed leading edge vortices. Surface flow visualizations illustrate the good qualitative correlation between the PowerFLOW simulations and the experiments. The traces of both the primary and secondary vortices are clearly visible on the surface shear lines of the computation and compare very well to the oil flow image. This indicates that the primary

vortex is captured correctly and its interaction with the wall boundary layer is also accurately reproduced.

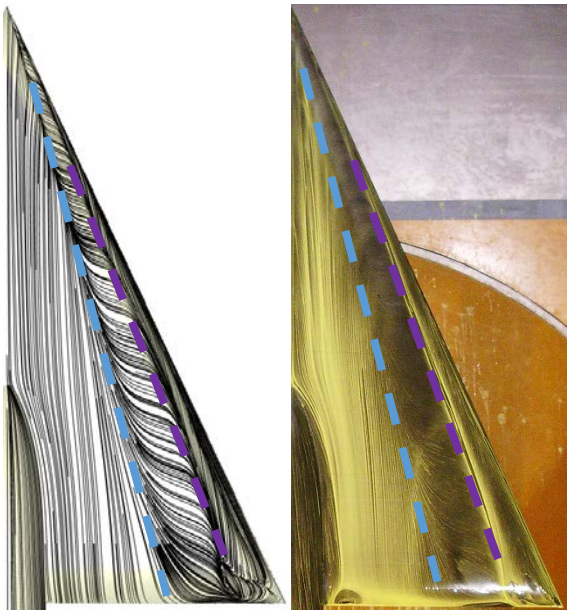

Figure 12-1 VFE-2 at α=13°, medium mesh. Surface flow visualization PowerFLOW (left) and experiment [2] (right). Blue line shows reattachment of primary vortex, purple line indicates detachment of secondary vortex.

The correct prediction of the location of the vortical structures is also observed in Figure 12-2, which shows a pressure coefficient (Cp) distribution resolution study for this configuration at two representative sections in the top row and standard deviation Cp distribution in the bottom row. Four grids are used: Very Coarse, Coarse, Medium, and Fine, which are refined by a factor of 1.5 for linear element size. The figures show planes at constant x/c (streamwise coordinate over wing chord), where η is the non-dimensional local span. Although a small change is observed at 95% of the chord, Cp results are fairly consistent with grid refinement. Standard deviation Cp shows some grid dependency, but medium and fine results are in good agreement with each other and experimental data. Hence, the medium grid is used for the remainder of this section analyses.

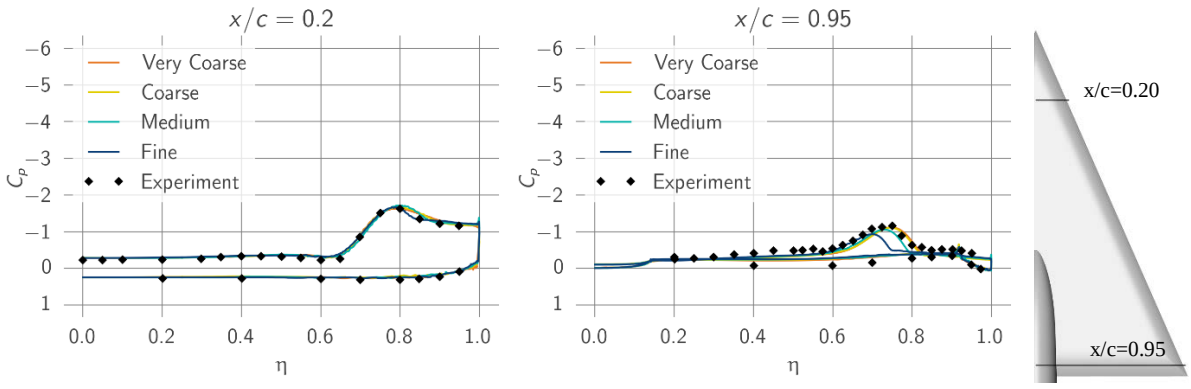

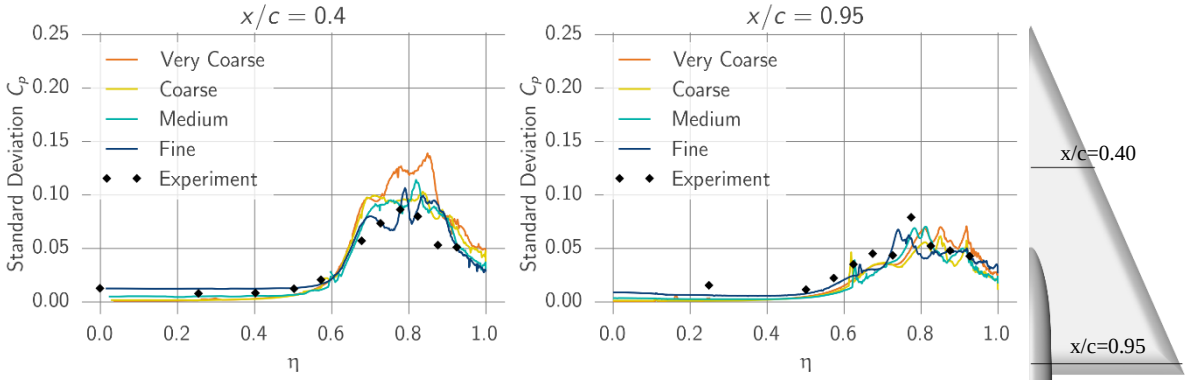

Figure 12-2 VFE-2 at α=13°. Cp distributions at two different streamwise sections (top) and standard deviation Cp distribution at two different sections (bottom). Experimental data from [2].

Figure 12-3 shows similar data to Figure 12-2, but at the much higher angle-of-attack of 23°. Simulation data matches the experiment very closely, with a slight underprediction of the secondary vortex footprint.

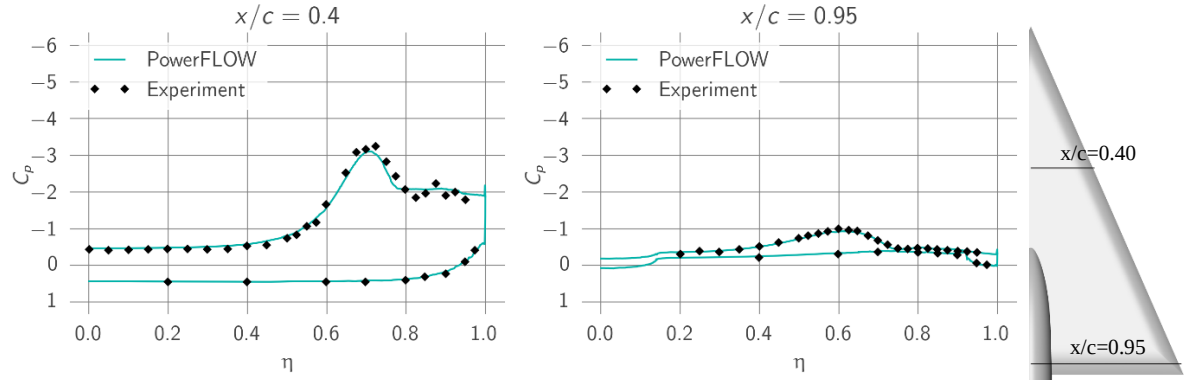

Figure 12-3 VFE-2 at α=23°. Cp distributions at two streamwise sections. Experimental data from [2].

Simulation results at 13° and 23° angle-of-attack are compared to experiments [2] for drag, lift, and moment coefficients (CD, CL, Cm) in Table 1. The values compare generally well with each other which is consistent with the surface pressure plots seen in Figure 12-2 and Figure 12-3.

Table 1: Comparison of experimental [2] and numerical force coefficients.

	AoA 13°		AoA 23°	
	Experiments	**PowerFLOW**	**Experiments**	**PowerFLOW**
C_D	0.125	0.113	0.385	0.382
C_L	0.587	0.518	0.977	0.948
C_m	0.075	0.0868	0.190	0.197

3.2 SACCON CONFIGURATION

In Figure 12-4, simulation results are shown for the SACCON configuration [17] with the combined rounded and sharp leading edge and including the support sting. A visualization of mean flow structures (λ_2) is documented in this figure for several relevant angles-of-attack, illustrating the complex flow topology including leading edge separation, vortex roll up, and separations, all captured by the method. Figure 12-5 depicts surface pressure distributions along with shear lines for the same angles. Both figures complement each other in understanding the behavior at these angles. At 10° the flow is mostly attached, with small wing tip separations and primary vortices that roll back at the wing root. At 15° the wing tip separation increases and stronger vortices are visible at the leading edges, running back at geometrical discontinuities. The flow at the mid-span seems to be fully attached, without a leading edge vortex. At 18° the wing tip separation develops into a large detachment of the primary vortex on the outboard wing, which moves inboard, with no fully attached leading edge flow at this point. This separation quickly moves inboard as the vortex breaks up, and at 20° it is close to the wing root. At 22° the separation is not moving inboard at the same rate, but the surface images show that it is difficult to separate the inboard and outboard leading edge vortices. As the angle increases to 28°, the primary vortex on the aircraft nose breaks up and detaches, with the wing now being completely stalled.

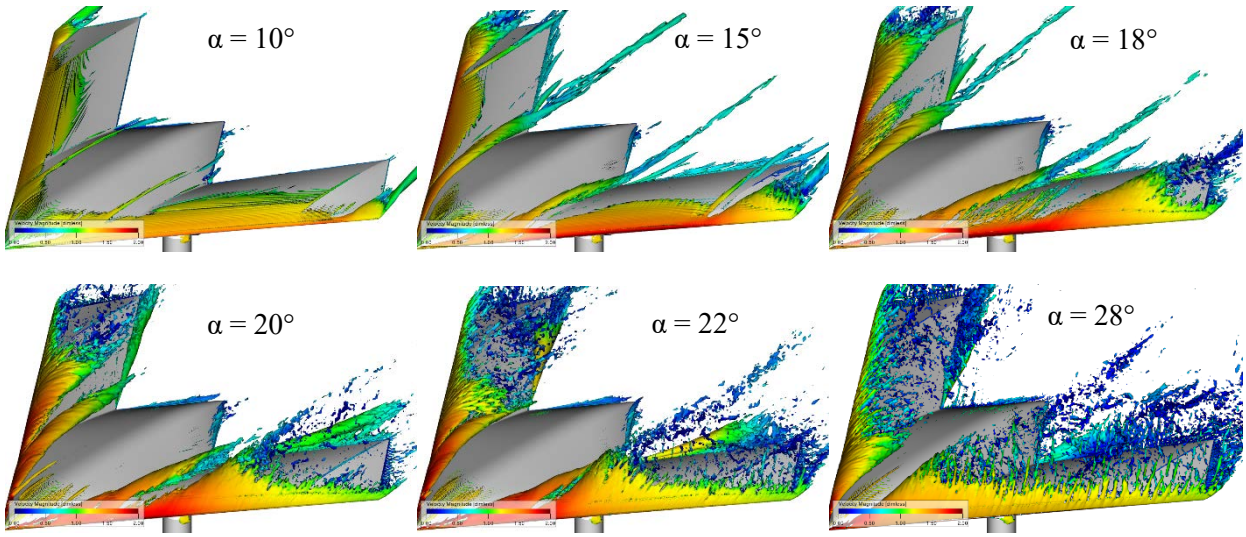

Figure 12-4 SACCON model, isosurfaces of λ_2 colored by velocity magnitude at several angles-of-attack.

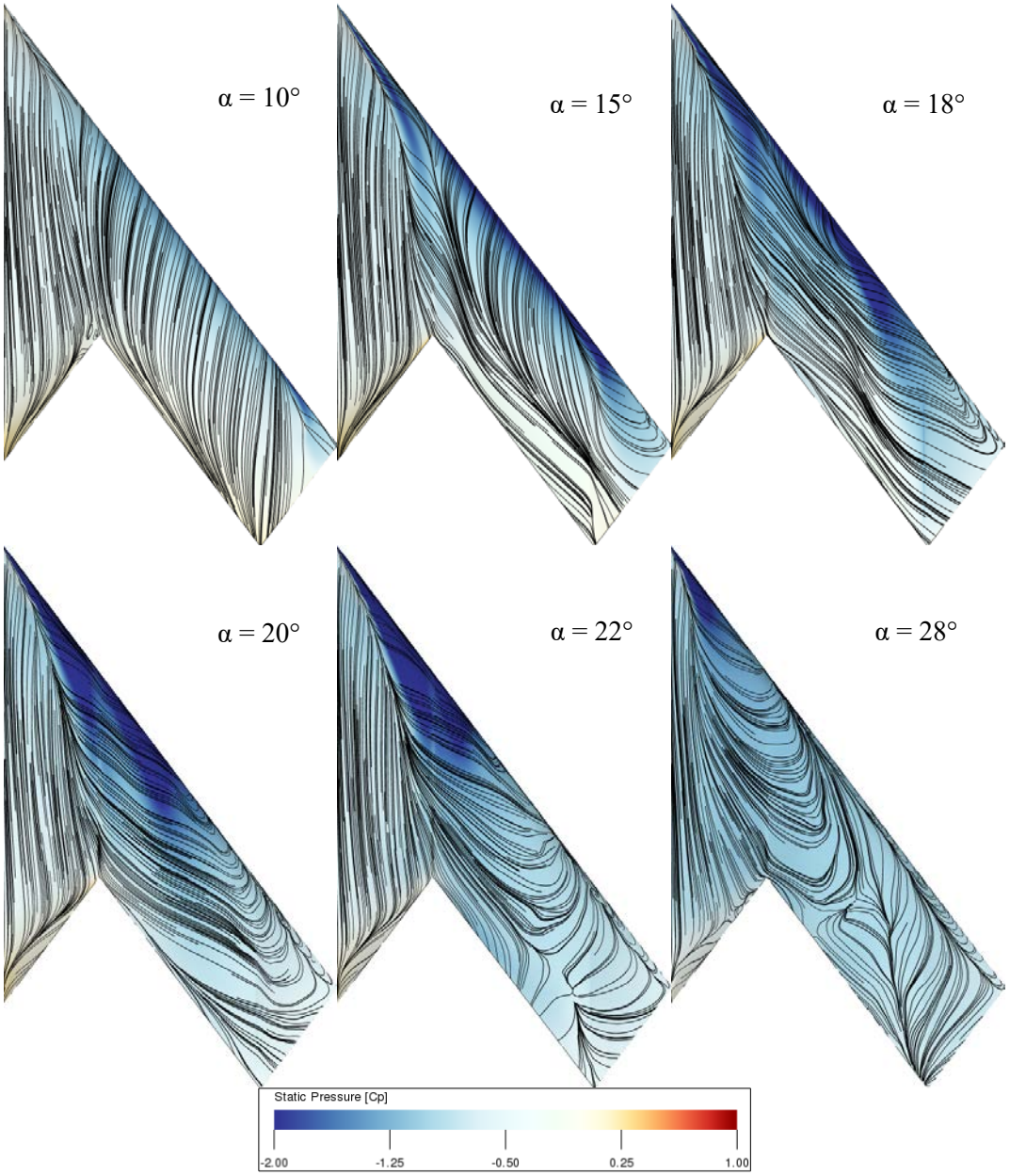

Figure 12-5 SACCON model, static pressure on the surface along with shear lines at several angles-of-.attack.

A comparison to experimental values is given for the lift and pitching moment coefficients in Figure 12-6. A very good match of the lift curve can be seen, even up to the highest angles-of-attack where the flow is highly separated. The pitching moment is showing some under-prediction for most angles, which is in line with the results presented in [18]. More importantly, the location and depth of the pitch-break starting at around α=16° is captured very well, indicating that the vortex behavior and the underlying flow physics are captured correctly. This has important implications when considering using simulation results for stability and control purposes. The highly non-linear behavior of C_M between 15° and 20° is explained by the separation and vortex break-up trends documented in Figure 12-4.

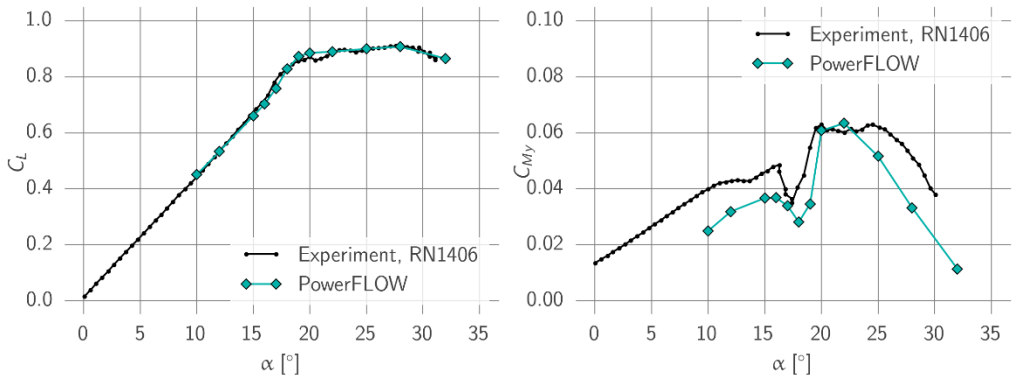

Figure 12-6 SACCON model, integrated lift (left) and pitching moment (right). Experimental data taken from [18].

In order to perform a more detailed comparison to experiments, surface pressure distributions are shown in Figure 12-7. Both sides of simulations and experiments are mirrored, so that only half of the span is shown. Some of the plots show two lines, indicating an asymmetry in the simulations. This is likely due to insufficient statistical convergence. The leading edge vortex generated at the nose and identified as a peak in the pressure distribution on the suction side seems to be more pronounced in simulation compared to experiment. The movement of the vortex as well as the plateau of pressure is generally well captured. The appearance of a second tip vortex for the angle-of-attack 17° is present as a second hump in the pressure distribution at the downstream section. This is however close to separation as can be seen at the higher angle-of-attack 22°. Overall the physical mechanisms associated with the vortex dynamics and separation mechanisms are qualitatively well captured and quantitatively in fair agreement. Further resolution studies are planned to be conducted for this configuration to determine the impact of added local resolution resolving more the vortex cores and potentially changing slightly their dynamics.

The unsteady nature of the current simulations allows one to check more than mean flow properties. With that in mind, Figure 12-8 examines standard deviation pressure over the upper surface of the aircraft, with the same isosurfaces seen in Figure 12-4 shown in transparent grey. This analysis highlights regions have the highest fluctuations on the surface and are related to the vortex meandering and interaction with separated flow regimes producing high level of unsteadiness. The unsteadiness is also present in force and moment coefficients and it was found that that the standard deviation of these quantities grow with angle-of-attack. In the images depicted in Figure 12-8 it can be seen that two main regions of high unsteadiness are present for this configuration. While at angle-of-attack 15°, just before the non-linear pitching moment behavior, the level of unsteadiness inboard and outboard are of similar magnitude, the behavior at 18° changes and higher fluctuations are documented at the outboard wing region. Separated flow regimes at higher angles-of-attack are moving the vortices inboard and hence moving the region of unsteadiness on the surface inboard. This could indicate that 18° and the angles-of-attack around the pitch moment non-linearity are prone to roll vibrations.

The mean and instantaneous flow field at 15° angle-of-attack is shown in Figure 12-9. This is essentially the same analysis as done in Figure 12-4, however showing the instantaneous data as well. The coherent vortices shown on the left are shown to actually consist of a large number of small resolved flow structures, see on the right, causing the observed unsteadiness in the pressure field and hence force and moment coefficients. This highlights the scale resolving capability of the numerical method and the difference between the mean flow and the real aerodynamics of such aircraft.

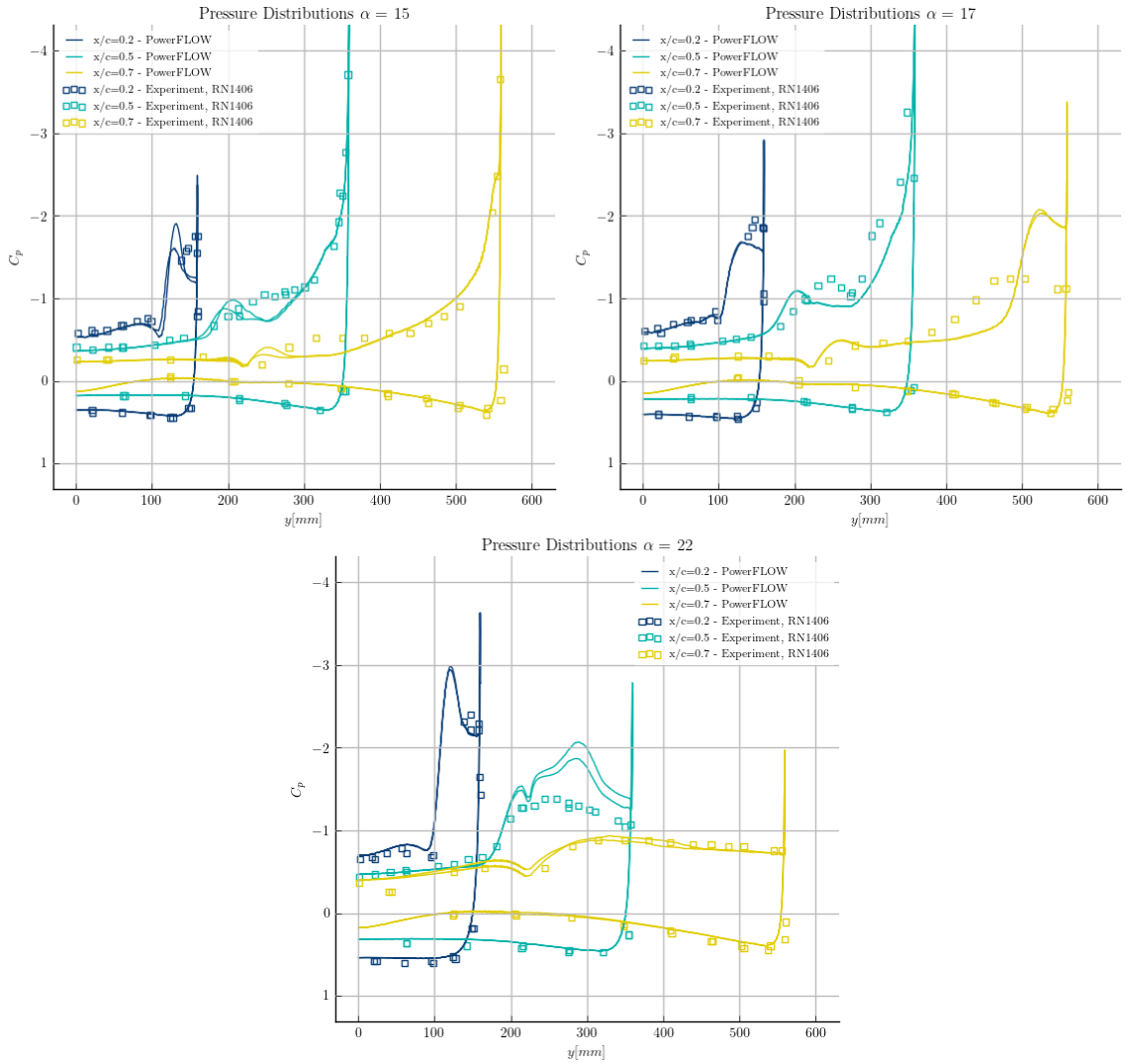

Figure 12-7 SACCON model, Cp distributions (right side and mirrored left side) for three angles-of-attack and three streamwise sections [18].

Finally, Figure 12-10 shows several mean flow slices along the aircraft chord documenting the behavior of the underlying turbulence modelling approach. The top left image shows vorticity magnitude, where a coherent vortex can be seen travelling over the wing-fuselage junction. The top right image shows how eddy viscosity has its maximum values inside the boundary layer and is relatively small in the vortex core, particularly on the second slice in the wing-fuselage junction. This behavior is especially crucial for allowing vortex cores to evolve and maintain their strength without the typical artificial dissipation associated with turbulence models not correctly modeling vortex cores. The bottom left image shows the modeled turbulence kinetic energy, which has a very similar behavior to the eddy viscosity. The bottom right image shows the resolved turbulence kinetic energy, which shows high fluctuations associated with the vortex flow motion. It is relevant to note that the resolved turbulence kinetic is shown in a range 50 times larger than the modeled one, indicating that the fluctuations in the vortical and separated flow regions are significantly more resolved than they are modeled.

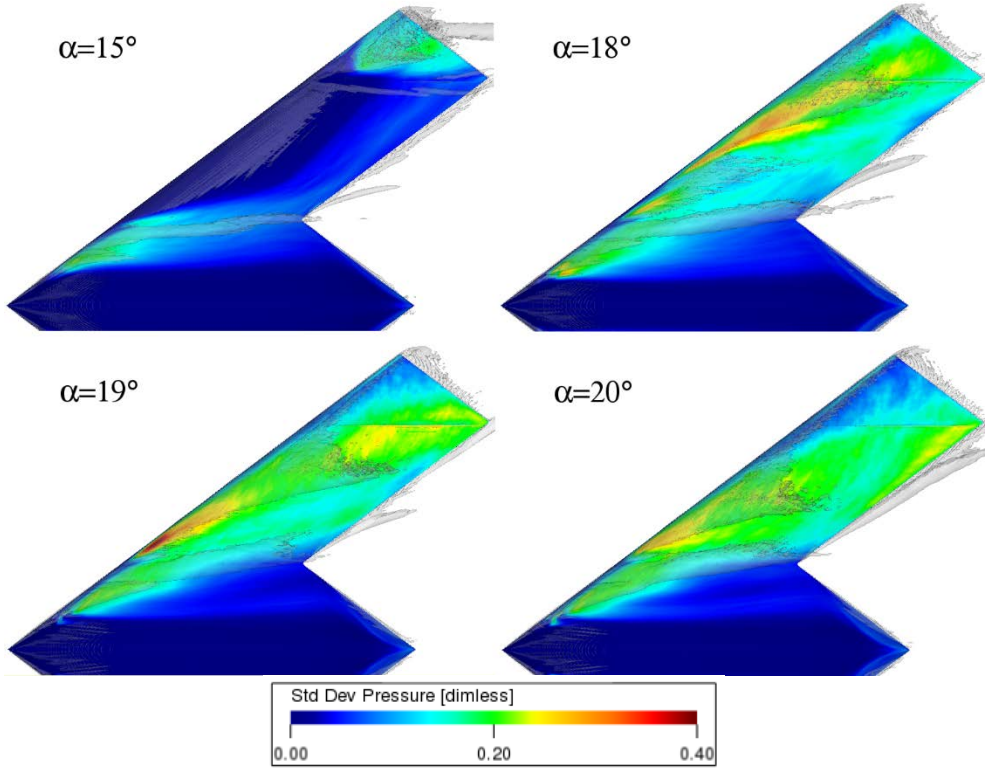

Figure 12-8 SACCON model, standard deviation pressure and isosurfaces of λ_2 at several angles-of-attack.

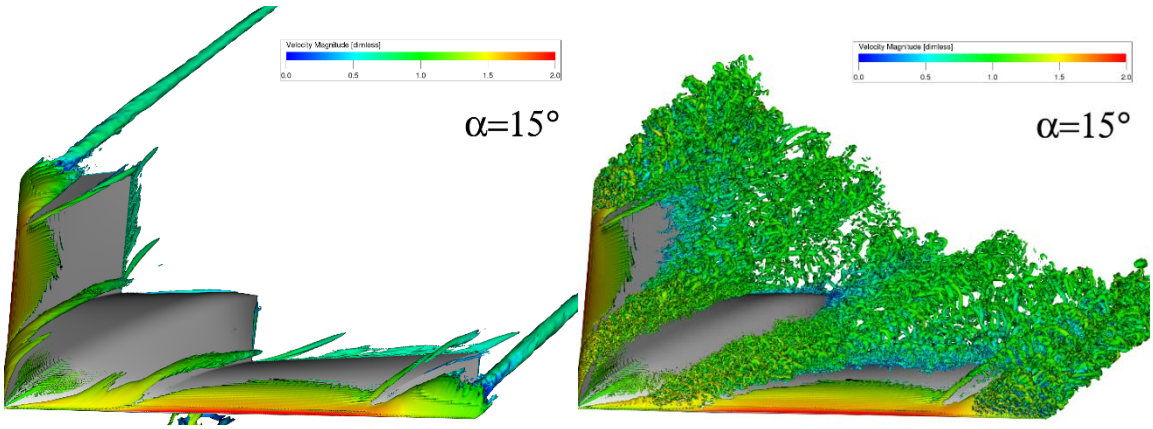

Figure 12-9 SACCON model, isosurfaces of mean (left) and instantaneous (right) λ_2 colored by velocity magnitude at 15°.

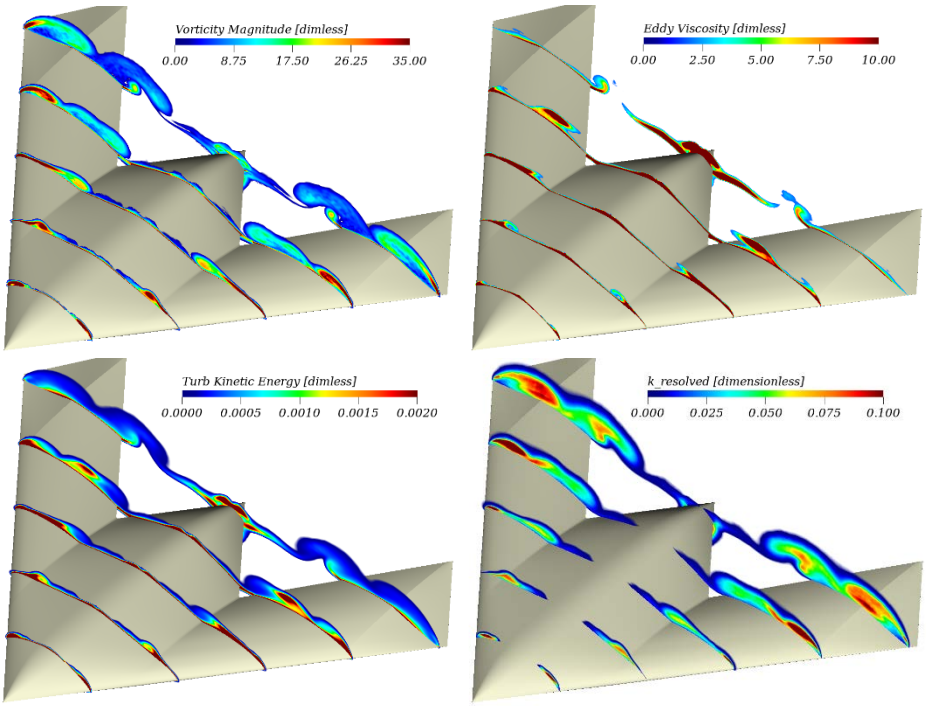

Figure 12-10 SACCON model, slices showing vorticity magnitude (top left), eddy viscosity (top right), modeled turbulence kinetic energy (bottom left), and resolved turbulence kinetic energy (bottom right) at 18°.

4.0 SUMMARY AND OUTLOOK

The Lattice Boltzmann-based CFD tool PowerFLOW was employed for vortex dominated flows at conditions with attached and massively separated flow. Two configurations with high leading edge sweep are considered, the VFE-2 and the SACCON. Results correlate well to experiments in terms of qualitative flow visualization as well as quantitative pressure distributions and integrated forces, even in the range of highly separated flow close and beyond C_{Lmax}. The intricate flow behavior of the generated vortical system reflected in the non-linear pitching moment evolution with angle-of-attack is captured accurately in simulation. The ability to accurately predict and directly simulate separated unsteady turbulent flows is one of the reasons why the numerical method is demonstrating a predictive capability for these type of flows on delta wings not only for averaged flow quantities but can also provide insights into the unsteady and associated flow induced vibration effects. Together with the proven capability of PowerFLOW to handle arbitrarily complex geometries under highly unsteady flow conditions, the current results indicate a path towards simulating complex delta wing aircraft in realistic environments.

5.0 ACKNOWLEDGEMENT

The authors would like to thank HLRS (Höchstleistungsrechenzentrum) Stuttgart for their support of the VFE2 computations under the grant DWLBM.

6.0 REFERENCES

[1] J. Slotnick, A. Khodadoust, J. Alonso, D. Darmofal, W. Gropp, E. Lurie and D. Mavriplis, "CFD Vision 2030 Study: A Path to Revolutionary Computational Aerosciences," 2014

[2] T. G. AVT-113, "Understanding and Modeling Vortical Flows to Improve the Technology Readiness Level for Military Aircraft," 2009.

[3] R. M. Cummings and A. Schütte, "An Integrated Computational/Experimental Approach to UCAV Stability & Control Estimation: Overview of NATO RTO AVT-161," in *28th AIAA Applied Aerodynamics Conference*, 2010.

[4] H. Chen, C. Teixeira and K. Molvig, "Digital Physics Approach to Computational Fluid Dynamics: Some Basic Theoretical Features," *International Journal of Modern Physics C*, vol. 8, pp. 675-684, 1997.

[5] S. Chen and G. D. Doolen, "Lattice Boltzmann Method for Fluid Flows," *Annual Review of Fluid Mechanics*, vol. 30, pp. 329-364, 1998.

[6] A. F. P. Ribeiro, D. Casalino, E. Fares and M. Choudhari, "Direct Numerical Simulation of an Airfoil with Sand Grain Roughness on the Leading Edge," 2016.

[7] M. Khorrami, R. Mineck, C. Yao and N. Jenkins, "A Comparative Study of Simulated and Measured Gear-Flap Flow Interaction," in *21st AIAA/CEAS Aeroacoustics Conference*, 2015.

[8] B. Koenig, E. Fares, M. Murayama and Y. Ito, "PowerFLOW Simulations for the Third AIAA High-Lift Prediction Workshop," in *2018 AIAA Aerospace Sciences Meeting*, 2018.

[9] D. Singh, A. F. Ribeiro, B. König and E. Fares, "Lattice Boltzmann Simulations of a Supersonic Cavity," in *35th AIAA Applied Aerodynamics Conference*, 2017.

[10] E. Fares, B. Duda and M. R. Khorrami, "Airframe Noise Prediction of a Full Aircraft in Model and Full Scale Using a Lattice Boltzmann Approach," in *22nd AIAA/CEAS Aeroacoustics Conference*, 2016.

[11] B. König, E. Fares, P. Ravetta and M. R. Khorrami, "A Comparative Study of Simulated and Measured Main Landing Gear Noise for Large Civil Transports," in *23rd AIAA/CEAS Aeroacoustics Conference*, 2017

[12] H. Chen, "Volumetric formulation of the lattice Boltzmann method for fluid dynamics: Basic concept," *Physical Review E*, vol. 58, pp. 3955-3963, 1998.

[13] H. Chen, S. Chen and W. H. Matthaeus, "Recovery of the Navier-Stokes equations using a lattice-gas Boltzmann method," *Physical Review A*, vol. 45, pp. R5339-R5342, 1992.

[14] H. Chen, S. Kandasamy, S. Orszag, R. Shock, S. Succi and V. Yakhot, "Extended Boltzmann Kinetic Equation for Turbulent Flows," *Science*, vol. 301, pp. 633-636, 2003.

[15] E. Fares, B. Duda, A.F.P. Ribeiro, B. Koenig, "Scale-resolving simulations using a lattice Boltzmann-based approach", *CEAS Aeronautical Journal*, 2018.

[16] T. D. Loeser, D. D. Vicroy and A. Schütte, "SACCON Static Wind Tunnel Tests at DNW-NWB and 14´x22´ NASA LaRC," in *28th AIAA Applied Aerodynamics Conference*, Chicago, Illinois, 2010.

[17] D. Vallespin, A. D. Ronch, K. Badcock and O. Boelens, "Validation of Vortical Flow Predictions for a UCAV Wind Tunnel Model," in *28th AIAA Applied Aerodynamics Conference*, Chicago, Illinois, 2010.